HHS Public Access

Author manuscript

Nat Commun. Author manuscript; available in PMC 2014 November 15.

Published in final edited form as:

Nat Commun. ; 5: 3699. doi:10.1038/ncomms4699.

Transmission from the dominant input shapes the stereotypic ratio of photoreceptor inputs onto horizontal cells

Takeshi Yoshimatsu[1], **Philip R. Williams**[1,2], **Florence D. D'Orazi**[1], **Sachihiro C. Suzuki**[1], **James M. Fadool**[3], **W. Ted Allison**[4], **Pamela A. Raymond**[5], and **Rachel O. Wong**[1,*]

[1]Department of Biological Structure, University of Washington, 1959 NE Pacific Street, Seattle, Washington 98195, USA

[2]Institute of Neuronal Cell Biology, Technische Universität München, Biedersteiner Street 29, D-80802 München, Germany

[3]Department of Biological Science and Program in Neuroscience, The Florida State University, 600 W College Avenue, Tallahassee, Florida 32306, USA

[4]Departments of Biological Sciences and Medical Genetics, University of Alberta, CW 405, Edmonton, Alberta T6G 2E9, Canada

[5]Department of Molecular, Cellular, and Developmental Biology, University of Michigan, 830 N University Avenue, Ann Arbor, Michigan 48109, USA

Abstract

Many neurons receive synapses in stereotypic proportions from converging but functionally distinct afferents. However, developmental mechanisms regulating synaptic convergence are not well understood. Here we describe a heterotypic mechanism by which one afferent controls synaptogenesis of another afferent, but not vice-versa. Like other CNS circuits, zebrafish retinal H3 horizontal cells undergo an initial period of remodeling, establishing synapses with UV and blue cones while eliminating red and green cone contacts. As development progresses, the horizontal cells selectively synapse with UV cones to generate a 5:1 UV-to-blue cone synapse ratio. Blue cone synaptogenesis increases in mutants lacking UV cones, and when transmitter release or visual stimulation of UV cones is perturbed. Connectivity is unaltered when blue cone transmission is suppressed. Moreover, there is no homotypic regulation of cone synaptogenesis by neurotransmission. Thus, biased connectivity in this circuit is established by an unusual activity-dependent, unidirectional control of synaptogenesis exerted by the dominant input.

*Corresponding author, wongr2@u.washington.edu.

Author contributions

T.Y., P.R.W., F.D.D. and R.O.W. conceived the study. T.Y., P.R.W. and F.D.D. performed experiments. T.Y. generated *Tg*(*sws1:TeNT*) and *Tg*(*sws2:TeNT*) transgenic animals. W.T.A. and P.A.R. provided *Tg(sws2:mCherry)* transgenic fish and J.M.F. provided *lor* mutant fish. S.C.S. designed the *thrb* morpholino. T.Y., P.R.W., F.D.D. and R.O.W. wrote the paper and all authors commented on the manuscript.

Competing financial interests

The authors declared no competing financial interest

INTRODUCTION

The output of a neuron is shaped by many factors, including the properties and stereotypic patterning of the synaptic connections it receives from a diversity of cell types. Our understanding of the developmental mechanisms responsible for generating proper wiring patterns have largely come from circuits where distinct afferent types innervate separate parts of the dendritic arbor[1,2]. For example, hippocampal CA3 neurons are contacted by large mossy fibers on their apical dendrites, proximal to the cell body, whereas entorhinal cortical projections contact the distal dendrites[3]. A number of molecules targeting axons to the appropriate compartment of the postsynaptic cell have now been identified[4,5,6]. By contrast, we have a much more limited understanding of the mechanisms that generate stereotypic patterns of synaptic convergence in circuits where functionally distinct inputs intermingle on the dendritic arbor[7]. Here, we investigated the cellular interactions that control the connectivity of two functionally disparate presynaptic cell types whose connections overlap on the dendritic arbor of the postsynaptic cell.

Like other parts of the nervous system, circuits in the vertebrate retina demonstrate a great deal of synaptic convergence and divergence[8]. Previous ultrastructural reconstructions[9,10] and recent light microscopy approaches[11,12] suggest that retinal neurons generally make a stereotypic number of synapses with each of their input types yet the mechanisms generating these patterns are not known. Complete circuit reconstruction is particularly tractable in the relatively small zebrafish retina, and many transgenic lines suitable for *in vivo* reconstruction are available. We focused on a simple but essential circuit in the outer retina, comprising cone photoreceptors and horizontal cells (HC), to gain an understanding of the cellular interactions responsible for setting up the appropriate synapse ratio of converging inputs.

There are four types of cones in the zebrafish retina[13,14], each with a peak sensitivity to either ultraviolet (UV), short (blue), medium (green) or long (red) wavelength light. In adult zebrafish, there are three types of cone HCs, classified according to their morphology and cone connectivity patterns[15,16]. H1 HCs contact red, green and blue cones whereas H2 HCs contact blue, green and UV cones. H1 and H2 HCs cannot be readily distinguished by their morphology. In contrast, H3 HCs can be recognized morphologically, and their circuitry is relatively simple because they contact only two cone types, UV and blue cones[16,17]. We show here that UV and blue cones form a stereotypic synaptic convergence ratio of about 5:1 with the H3 HCs. To determine whether the synaptic convergence ratio is dictated by the ratio of UV:blue cone number within the dendritic field of the H3 HC, we altered UV cone numbers prior to synaptogenesis with HCs, using mutant fish and morpholino approaches. To explore the role of synaptic activity in establishing the UV:blue cone synapse ratio, we generated transgenic animals in which UV or blue cone transmitter release is selectively perturbed. Because H3 HCs connect with cones largely after cone opsins are expressed, we also investigated the role of sensory experience in defining the cone connectivity pattern of H3 HCs. Together, our observations reveal a previously unknown *in vivo* cellular mechanism, by which one input type uses an activity-dependent process to control the number of synapses the other input type makes with their common postsynaptic partner.

RESULTS

Morphological identification of H3 HCs during development

HCs in zebrafish larval retina were labeled by expression of fluorescent protein under the Cx55.5 promoter[18] (Fig. 1a–c). As in adult zebrafish[15], H1 and H2 (H1/2) cone HCs in larvae could not be readily distinguished from each other by their dendritic morphology alone, whereas H1/2 and H3 HCs appeared morphologically distinct (Fig. 1a–c). We found that shortly after HC genesis, H3 HCs showed lower densities of dendritic tips and larger dendritic field sizes than H1/2 HCs (Fig. 1d). These morphological differences persisted in older larvae (Supplementary Fig. 1). As in adult zebrafish, we observed that larval HCs made invaginating dendritic contacts with cone photoreceptor axonal terminals, or pedicles. The dendritic tips of the HCs were apposed to presynaptic ribbon structures (Fig. 1e), and contained ionotropic glutamate receptors (Fig. 1f) as previously demonstrated[19]. We define here an HC-cone synapse as the invagination of a single dendritic tip within an individual cone pedicle.

H3 HCs preferentially contact UV and blue cones

Adult H3 HCs only contact UV and blue cones[16], but whether H3 HCs also demonstrate this wiring specificity during development is not known. In order to obtain the connectivity patterns of developing H3 HCs, we coinjected pCx55.5:Gal4 and pUAS:MXFP plasmids into double transgenic fish in which UV cones (*sws1:GFP*) and blue cones (*sws2:mCherry*) express different color fluorescent proteins (FP) under cone type-specific promoters. We obtained confocal reconstructions of H3 HCs at various larval ages, from 3.5 days postfertilization (dpf), around the onset of synaptogenesis in the outer plexiform layer (OPL)[20], to 10.5 dpf, when visually guided behavior is well-established[21] (Fig. 2a). At all ages studied, H3 HCs contacted mostly UV and blue cones (Fig. 2b). On average, the number of UV cones contacted by an H3 HC increased with age ($p<0.01$; one-way ANOVA), whereas the number of blue cone synapses remained constant across time points ($p>0.05$; one-way ANOVA) (Fig. 2b).

We noticed that some dendritic tips were not apposed to the fluorescently labeled UV cones or blue cones, especially at 3.5 dpf (Fig. 2, undefined tips). To determine whether fluorescent protein is not yet expressed by all UV or blue cones at early ages, we performed immunostaining with anti-UV- or blue-opsin antibodies. We found that at 3.5 dpf, 19 ± 3% (n=4 eyes) of UV-opsin-positive cones lacked *sws1:GFP* expression, but by 10 dpf, 99 ± 0.3% (n=4 eyes) were visualized by GFP expression (Supplementary Fig. 2a,b). All blue-opsin-positive cones showed *sws2:mCherry* expression at all ages examined (Supplementary Fig. 2a,b). Because of the incomplete transgene expression at early ages, the number of UV cones contacted by immature H3 HCs is likely to be greater than that quantified based on *sws1:GFP* labeling alone. We adjusted our measurements to account for the fraction of unlabeled UV cones, and found that the estimated number of unlabeled UV cone contacts (1.68 ± 0.31) was still less than the average number of ‘undefined’ tips (5.83 ± 0.87) at 3.5 dpf (Supplementary Fig. 2c and Fig. 2b). We wondered whether some of the undefined tips were contacting red and green cones, and to test this we performed immunostaining with the

zpr-1 antibody that labels both these cone types[22]. Indeed we found that H3 HCs transiently contacted a few red and green cones before 5.5 dpf (Supplementary Fig. 3).

Taken together, our data reveal two key characteristics of the development of cone synaptic convergence onto H3 HCs. First, elimination of red and green cone contacts contributes to the H3 HC's mature connectivity pattern, which comprises synapses with only UV and blue cones. Second, the UV:blue cone synapse ratio increases with maturation.

Selective synaptogenesis underlies UV cone dominance

The synaptic bias towards UV cones may be a consequence of a greater abundance of UV cones compared with blue cones in larval zebrafish[23]. We counted the number of UV cones and blue cones present within the retina from 3.5 to 10 dpf (Supplementary Fig. 2a,b), and compared these counts with the ratio of UV:blue cones that the H3 HC contacted (Fig. 3a). We found that the ratio of UV:blue cone synapses exceeds the relative abundance of UV and blue cones, suggesting that cone type 'availability' does not fully account for the biased connectivity with UV cones.

How is the bias towards UV cones established over time? The dendritic field size of H3 HCs increases with age ($p<0.02$; one-way ANOVA) (Fig. 3b), suggesting that H3 HCs are likely to add synapses onto the distal dendrites between 3.5 and 10 dpf. To further assess whether the growing H3 HC arbor preferentially contacts UV cones, we compared the location of UV and blue cone contacts on the dendritic arbor of H3 HCs at different ages, as illustrated in Figure 3c. We overlaid a circle with an area equivalent to the average dendritic field area of H3 HC dendritic arbors at 3.5 dpf, and compared the average number of UV and blue cone contacts within and outside this circle across ages. This circle approximates the arbor of the cell at the earliest stage examined (3.5 dpf), whereas dendrites outside the circle are likely to be added subsequently. H3 HCs added UV cone contacts within the circle up to 5.5 dpf, contacting nearly all of the nearby UV cones. There was no further increase in UV contacts within this circle up to 10 dpf. However, H3 HCs appeared to add UV cone contacts continuously to the peripheral arbor from 3.5 to 10 dpf. In contrast to UV cones, there was no addition of blue cone contacts after 5.5 dpf to the peripheral arbor, suggesting that H3 HCs only form contacts with blue cones early in circuit formation. In fact, when we compared the contacts on the same cell a day apart (96 and 120 hpf), we found that UV contacts were added only to the distal dendrites (n=3; Supplementary Fig. 4). Thus, preferential addition of UV cones to the peripheral arbor as the dendrites grow during later stages of development underlies the progressive increase in the UV:blue cone synapse ratio.

The relatively constant number of blue cones contacted across ages may result from H3 HCs failing to attempt to form new synapses with this cone type after 3.5 dpf. Alternatively, H3 HCs may actively add contacts with blue cones after 3.5 dpf but eliminate these contacts. To distinguish between these possibilities, we performed timelapse imaging of H3 HCs in the background of labeled UV cones (*Tg*(s*ws1:GFP*) or blue cones (*Tg(sws2:GFP*) for 24 hours, beginning at 3.5 dpf (Fig. 4). Throughout the period of imaging, UV cone contacts were both added and eliminated (Fig. 4a and c) but there was a net increase in the number of UV cones contacted by the end of the recording period (Fig. 4d). In contrast, H3 HCs only occasionally added or eliminated blue cone contacts (Fig. 4b and c), resulting in almost no

net change in synapses with blue cones within this time period (Fig. 4d). In summary, within the 24 hour period of recording starting at 3.5 dpf, H3 HCs gained UV cone synapses, but no or relatively few blue cone contacts. Therefore, H3 HCs fail to increase their number of connections with blue cones over time because they do not actively engage blue cones in synaptogenesis after 3.5 dpf.

H3 HCs increase connections with excess UV cones

To gain insight into the cellular interactions that regulate the balance of inputs amongst different cone types onto the H3 HC, we first asked whether increasing the density of UV cones in the retina affects their connectivity with the H3 HC. We therefore analyzed H3 HC connectivity in animals in which a morpholino directed against thyroid hormone receptor β2 (*thrb* morphant) causes a doubling in UV cone density without changing blue cone density[24] (Fig. 5a–d). Figure 5e–h shows an example of an H3 HC and its connectivity in the *thrb* morphant retina at 5.5 dpf. Compared with controls, H3 HCs in the morphant increased their total number of dendritic tips, without changing their dendritic field size (Fig. 5 i,j). The increase in total tip number was driven by an increase in synapses with UV cones (Fig. 5k). By 10 dpf, morphant H3 HCs contacted the majority of the UV cones within their dendritic fields, as in wildtype animals (Fig. 5l). Thus, the number of UV cones an H3 HC contacts is dependent on the number of available UV cones within the cell's vicinity. Despite significantly increasing their contact with UV cones, morphant H3 HCs contacted the same number of blue cones as morpholino controls (Fig. 5k). Therefore, during normal development, H3 HCs do not contact blue cones simply because there are insufficient UV cones available for attaining a desired total synapse number.

UV cone depletion increases H3 connectivity with blue cones

We next asked whether decreasing UV cone density during development would affect the H3 HC's connectivity pattern. We crossed the *lor* mutant, in which the total number of UV cones in the retina is reduced without changing the total number of blue cones[25], into the background of the double transgenic, *Tg(sws1:GFP; sws2:mCherry*) (Fig. 6a–d). In the *lor* mutant, the few remaining UV cones appear in random patches across the retina (Fig. 6c). An example of an H3 HC and its connectivity pattern in the mutant at 5.5 dpf is provided in Figure 6e–h. There were no significant differences in H3 HC dendritic field size between the mutant and wildtype animals (Fig. 6i). However, H3 HCs increased contact with blue cones (Fig. 6k), resulting in only a small decrease in their total contact number compared with controls (Fig. 6j, k). H3 HCs thus contacted a significantly higher fraction of blue cones within their dendritic fields in the *lor* mutant (Fig. 6l).

Like in wildtype, H3 HCs in *lor* contacted nearly 100% of the available UV cones, but each H3 HC in *lor* experienced variable densities of UV cones within their dendritic field. In some cells, the dendritic tips that invaginated UV cones were enlarged (Fig. 6e), whereas in other cases, H3 HCs projected two tips into the same UV cone (Fig. 7a–c). A plot of the number of UV cone versus blue cone synapses for individual cells in *lor* at 5.5 dpf (Fig. 7d) shows that in *lor*, there is an inverse relationship between the number of UV cones contacted and the number of blue cones contacted. Thus, H3 HCs respond to a lack of UV cones by

modifying their dendritic contact area with available UV cones and by increasing their blue cone synapse number.

UV cone transmission regulates connections with blue cones

Our finding of a compensatory increase in blue cone contacts in the *lor* mutant suggests that the H3 HC's dominant partner type, UV cones, influence connectivity with the secondary partner type, blue cones. Is this regulation mediated by transmission from cones? To test this possibility, we generated transgenic fish in which tetanus toxin fused to cyan fluorescent protein (TeNT-CFP) is expressed in UV, blue, or both cone types, without changing their densities (Supplementary Fig. 5a). TeNT perturbs exocytosis[26] and thus reduces synaptic transmission. Figure 8a–l shows an example of an H3 HC and its connectivity pattern at 5.5 dpf from each of the TeNT transgenic lines. Reduction in transmission from UV, blue, or both cone types did not affect the dendritic field size of H3 HCs relative to controls (Fig. 8m).

However, the number of blue cones contacted by an H3 HC significantly increased when only UV cone transmission was perturbed (Fig. 8n). This resulted in a reduction in the UV:blue synapse ratio (Supplementary Fig. 6) and a larger percentage of blue cones within the field being contacted (Fig. 8o), similar to *lor* mutants (Fig. 6l). In contrast to *lor* mutants, H3 HCs maintained the same number of UV cone connections in *sws1:TeNT* retina as in control retina. Suppression of blue cone transmission alone did not alter the number of UV cone or blue cone contacts (Fig. 8n). Together, these manipulations of neurotransmission demonstrate that UV cone transmission regulates H3 HC connectivity with blue cones, but not with the UV cones themselves, and that blue cone transmission is not required for normal circuit formation. Moreover, in the absence of drive from either of the preferred cone inputs, H3 HCs do not reach out to zpr-1-immunopositive red or green cones (n=8; *sws1:TeNT*, n=5; *sws2:TeNT*), suggesting that partner choice is not dependent on neurotransmission from photoreceptors. However, when transmission from both UV and blue cones is suppressed, H3 HCs do show reduced contact with both cone types (Fig. 8n).

To ascertain whether the effects of UV cone transmission are light-dependent, we designed a morpholino against UV-opsin (*Opn1sw1*), rendering UV cones insensitive to UV light but allowing them to release neurotransmitter. Injection of *Opn1sw1* morpholino into single-cell fertilized eggs abolished all Opn1sws1 immunoreactivity but did not affect UV cone density (Supplementary Fig. 5b). As in *Tg(sws1:TeNT*) fish, H3 HCs in the *Opn1sw1* morphant demonstrated an increase in blue cone contact number without changing UV cone connectivity (Fig. 9), indicating that light-dependent transmission from UV cones normally modulates synapse number with blue cones.

DISCUSSION

It has long been appreciated that heterosynaptic modifications occur in CNS circuits in which functional changes in one input affects other inputs sharing the same postsynaptic cell[27,28,29]. Most of these past studies have focused on functional plasticity of mature synapses. Here, we show that in a developing retinal circuit, one input type regulates synaptogenesis of the other input through an activity-dependent, sensory-drive mechanism

(results summarized in Supplementary Fig. 6). Unlike synaptic plasticity in most circuits, the regulation of synaptogenesis is unidirectional, i.e. UV cone input on H3 HCs controls HC connectivity with blue cones, but not vice-versa.

Our analysis suggests that the stereotypic connectivity of H3 HCs is established during development through two processes. First, early in development, H3 HCs contact inappropriate partner types (red and green cones) in addition to UV and blue cones, but such errant contacts are rapidly eliminated. In this regard, H3 HCs establish specificity through an early phase of circuit refinement, which is also found in other vertebrate retinal circuits[30] as well as in many parts of the nervous system[31, 32]. The second phase of synaptogenesis commences at the onset of cone transmission, around 3 dpf[33], and during this stage the synapse ratio of UV:blue cones increases significantly. This bias arises from H3 HCs selectively forming synapses with UV cones while maintaining synapses with blue cones that were formed early on. Many other systems establish their mature connectivity patterns by pruning inappropriate connections and further refine by eliminating some connections with appropriate partners[28,31]. In contrast, H3 HCs achieve their biased connectivity towards UV cones largely by selectively increasing synaptic contact with UV cones, rather than by pruning excessive blue cone contacts.

The developmental increase in contact with UV cones cannot be accounted for by addition of newly generated UV cones within the field of HC dendritic arbor because cone genesis is complete prior to synaptogenesis with H3 HCs[20,34]. It is also unlikely that the relative availability of presynaptic cell types alone dictates H3 HCs' selective synapse formation with UV cones. Although UV cones outnumber blue cones by 1.5:1 at all larval stages examined, this ratio is far below the UV:blue cone synapse ratio of 5:1. Thus, H3 HCs increase synaptogenic preference for one of their two input types in the context of a stable population of presynaptic partners.

Mutant fish and morpholino approaches allowed us to investigate how the relative numbers of UV and blue cones prior to synapse formation impact the convergence ratio of the presynaptic partner types. Normally, an H3 HC connects with almost all of the UV cones within its dendritic field. However, observations based on the *thrb* morphants suggest that H3 HCs can increase the number of synapses they make with UV cones when more UV cones are available during development. This observation resembles previous findings in *nrl* knockout mice in which an excess of cones develop in the absence of rods, and the HCs increase their density of synaptic contact with cones[35]. Thus, across species, the number of available presynaptic partners can set the upper limit of the number of connections they form with the postsynaptic cell. However, in zebrafish, this does not apply to synapses with secondary inputs because H3 HCs normally contact only about half of the blue cones within their dendritic fields.

We found that the availability of the dominant input type can also affect the connectivity of the secondary input type. Connectivity with blue cones increases above normal levels when UV cone numbers are decreased, as in the retinas of the *lor* mutants. Compensatory changes in one input type when the other type is absent have been previously observed. Notably, degeneration of parallel fibers results in the expansion of the dendritic territory occupied by

climbing fibers on Purkinje cell dendrites, and vice versa[36,37,38]. Is this compensatory change aimed at reaching a fixed, total number of synapses? We do not find support for this mechanism in cone-H3 HC circuits, because the total number of synapses in the *thrb* morphant exceeds the control number. This suggests that in wildtype animals, the number of blue cone synapses is not regulated by a mechanism that sets the total number of synapses. Instead, blue cone synapse numbers are normally maintained at low levels, but can be increased when there are fewer favored synaptic partners available to H3 HCs. Finally, the number of blue cone contacts in the *thrb* morphant may remain unaltered because H3 HCs in the *thrb* morphant increase contact with supernumerary UV cones largely after synaptogenesis with blue cones.

A well-accepted mechanism that shapes neuronal connectivity patterns is activity-dependent competition[39,40,41]. Competition results in a 'winner take-all' scenario, in which connections with one input type are eliminated and synaptic territory is taken over by the other input type. Generally, the input that is relatively less active loses. Here, we showed that perturbing transmission from UV cones results in an increase in connectivity with blue cones, revealing an activity-dependent process. But, unlike activity-driven competitive mechanisms, the suppressed UV cones do not lose connectivity with the postsynaptic cell. This result resembles that observed when input from parallel fibers to Purkinje cells is blocked: the number of climbing fibers contacting the Purkinje cell is increased, but synapses with parallel fibers are maintained[42]. When climbing fiber input is perturbed instead, parallel fibers increase their innervation of the proximal dendrites of the Purkinje cells[43]. Together, these observations suggest that there is bidirectional influence on connectivity by both input types. In contrast, connections on H3 HCs are influenced unidirectionally by the activity of only one input; blocking blue cone transmission does not result in an increase in UV cone connectivity. Thus, we have uncovered a previously unknown mechanism that regulates the pattern of synaptic convergence onto an individual neuron, which engages an activity-dependent process that is dictated by only one afferent type, the dominant input.

Why does UV cone transmission affect blue cone connectivity and not vice versa? An obvious explanation is that UV cones provide the majority of the net photoreceptor drive onto H3 HCs. When synaptic drive is diminished, either by loss of UV cones or lack of UV cone transmission, H3 HCs may seek connections with other active cones as part of a compensatory response. Thus, loss of drive from the few blue cones would not be sufficient to trigger a compensatory response. Congruent with this hypothesis, a previous study of mixed hippocampal neuronal cultures from wildtype and mutant animals lacking the NMDA receptor subunit GluN1 demonstrated the presence of a threshold (> 50% inactive), only above which changes in connectivity were detected[44]. It is not clear, however, that a set threshold exists for the H3 HC-cone circuit because we find an inverse relationship between the number of blue cones and UV cones that are contacted by an individual H3 HC (Fig. 7d). We propose that the most parsimonious explanation is that specific loss of transmission from UV cones triggers a mechanism to recruit blue cone connections. We also noted that when all drive to H3 HCs is suppressed, both UV and blue cone connections decline. This is reminiscent of findings in mammalian retina, where blockade of transmission from all ON bipolar cells leads to an overall decrease in synaptic contact with ON retinal ganglion

cells[45]. Thus, a compensatory increase in connectivity with presynaptic cells may only occur when there are presynaptic partners that are still able to transmit.

As yet, our experiments do not directly reveal whether or not the postsynaptic cell mediates the heterotypic regulation of cone connectivity. It is known that photoreceptors are coupled by gap-junctions[46], and thus the relevant signals may be conveyed directly between cones. However, if the suppressive signal passes between cones via gap junctions, then we would not expect changes to blue cone connectivity in the *sws1:TeNT* retina, in which we interfered with the release of neurotransmitter without preventing the cones from responding to changes in illumination. Therefore, it is more likely that transmission from UV cones acts via a mechanism directly involving the H3 HC. Indeed, in cerebellar circuits it has been shown that Purkinje cells mediate the interactions between climbing fibers and parallel fibers that establish their respective synaptic territories[28]. Regardless of the exact 'postsynaptic' mechanism, our study clearly shows that synaptic convergence of each distinct input onto a sensory neuron is not necessarily independently regulated; instead, one input type can unidirectionally dictate the connectivity of the other.

METHODS

Transgenic and mutant zebrafish

Zebrafish were maintained and experiments conducted in accordance with University of Washington Institutional Animal Care and Use Committee guidelines. Fish were raised in an incubator with a transparent door in a room with a normal light cycle, typically lights on from 9 am to 11 pm. We used a combination of transgenic lines to visualize UV and/or blue cones by fluorescent protein (FP) expression. *Tg(sws1:GFP)*[47] labels UV cones, and *Tg(sws2:GFP)*[48] labels blue cones. As an additional method to visualize blue cones, a transgenic line was engineered to express mCherry in blue cones *Tg(sws2:mCherry)*[49]. To block neurotransmission from cones, we generated transgenic lines in which tetanus toxin light chain (TeNT) fused to CFP is expressed in UV (*Tg(sws1:TeNT*), or blue cones (*Tg(sws2:TeNT*). Transgenic lines were generated by plasmid injection with or without transposase RNA into fertilized eggs at the one-cell stage, and subsequent F1 generations were screened by FP expression.

For *in vivo* time-lapse imaging of the retina, we used the *roy orbison* mutant background[50] in which iridophores do not form. The cone innervation pattern of H3 HCs in the *roy orbison* mutant resembles that of wildtype fish (Supplementary Fig. 7).

The lots-of-rods (lor) mutant was isolated from N-ethyl-N-nitrosourea-induced mutant fish[25]. Homozygous *lor* mutant fish showed no obvious morphological phenotype except a decreased number of UV cones and an increased number of rod photoreceptors.

Plasmid generation

To visualize individual HCs, we used the pCx55.5:Gal4VP16 plasmid together with plasmids that express fluorescent protein tagged with membrane localization signal under the UAS promoter (pUAS:MXFP)[51]. MXFP represents MtdCerulean, MYFP or MtdTomato. pUAS:MtdCerulean plasmid was generated by inserting a tandem repeat

Cerulean coding region tagged with membrane localization signal under the UAS promoter. pUAS:MtdTomato plasmid was generated by replacing the YFP coding region from pUAS:MYFP plasmid with tdTomato.

To generate transgenic fish lines, we constructed pSws1:TeNT and pSws2:TeNT plasmids using the Gateway (Life Technologies) and Tol2 system[52]. Cone type-specific promoters were excised from *sws1:GFP*[47] and *sws2up3.2kb:EGFP* plasmids[48], and inserted into p5E plasmids. TeNT-CFP[45] was inserted into pME plasmid. Subsequent plasmids were subjected to a Gateway reaction together with p3E–polyA and pDestTol2pA.

Morpholinos

Morpholino sequences are 5'-CCTCTTACCTCAGTTACAATTTATA-3' (Standard control), 5'-CGAATTGAACGGCCCACGCGTCCAT-3' (*Opn1sw1*, Acc#; AF109373.1) and 5'-TCTAGAACTTGCAATACCTTTCTTA-3' (*thrb*, Acc#; AB759513).

Plasmid and morpholino injection

Plasmid and/or morpholino (Gene Tools, LLC) were diluted in 1X Danieau's solution (58 mM NaCl, 0.7 mM KCl, 0.6 mM $Ca(NO_3)_2$, 0.4 mM $MgSO_4$, 5mM HEPES, pH 7.6) with 0.1% phenol red to aid visualization of the injection bolus. Plasmid and/or morpholino solutions were injected into fertilized eggs at the one-cell stage. A pulled-glass micropipette loaded with injection solution was attached to a Picospritzer II (Parker) and anchored on a micromanipulator (Narishige) for small volume microinjections. Injection pressure was set to 10 psi and durations ranged from 100 to 300 ms. Total concentrations from 20 to 100 ng/μl for plasmids with and without 0.25 mM morpholino were injected. Injected eggs were maintained in 0.3X Danieau's in an incubator at 28°C. At 12–24 hpf, the medium was replaced with 0.3X Danieau's containing 0.2 mM Phenyl-thiourea (PTU) to prevent melanin synthesis. Embryos were maintained in this medium up to 5.5 dpf. For the following incubation, fish were raised without PTU and fed regularly.

In vivo imaging

Embryos at various stages were anesthetized with MS-222 (25–50 mg/l) in 0.3X Danieau's solution) and mounted in molten 0.5% low-melting-point agarose (type VII, Sigma) in 60 mm organotypic culture dishes (Falcon). After solidification of the agarose, fish were covered with 0.3X Danieau's solution containing 0.2 mM PTU and MS-222 (25– 50 mg/ml). Image stacks were acquired on a confocal microscope (FV1000, Olympus) or a custom-built two-photon microscope consisting a Ti-Sapphire tunable infrared laser (Spectra-Physics) at 850–915 nm. A 1.1 NA 60X water immersion objective lens with a refractive index correction collar was used (Olympus). Images were typically acquired with an XY resolution of 0.077 μm/pixel and 0.3 μm-thick Z slices. For time-lapse imaging, zebrafish embryos were released from agarose after each image acquisition period and returned to fish water without MS-222, so as to minimize the effects of anesthesia.

Immunohistochemistry and imaging wholemounts

Zebrafish were euthanized by icing, and then fixed in 4% paraformaldehyde (PFA) and 3% sucrose in 0.1M phosphate buffered saline (PBS), pH 7.4, for 25 min at room temperature.

For anti-Gria2/3 (GluR2/3) immunohistochemistry, fish were fixed in 3% PFA and 3% sucrose in PBS for 19 min at room temperature. Samples were washed three times for 5 min in PBS. Eyes were removed in PBS. Whole eyes were blocked in a solution containing 5% normal donkey serum and 0.5% TritonX-100 in PBS for 1–24 h and then incubated with primary antibodies. Primary antibodies included anti-GluR2/3 (rabbit, 1:300, Millipore), anti-UV-opsin (rabbit, 1:500, kindly provided by David Hyde), anti-UV-ospin (rabbit, 1:5000, kindly provided by Jeremy Nathans), anti-blue-opsin (rabbit, 1:5000, kindly provided by Jeremy Nathans) and zpr-1 (mouse, 1:100, ZIRC) were diluted in blocking solution. After incubating in primary antibody for 1–3 days at 4°C, samples were washed three times, 5 min each in 0.5% TritonX-100 in PBS and incubated for 3 hours with secondary antibody, DyLight 649 Donkey anti-rabbit or antimouse (1:500, Jackson ImmunoReseach) diluted in blocking solution. After three, 15 min washes with 0.5 % TritonX-100 in PBS, whole eyes were mounted in 0.5% agarose and coverslipped with Vectashield mounting medium (Vector). For H3 HC imaging, the eyes were oriented with the photoreceptor layer closest to the cover slip. For imaging of H3 HC dendritic tips with anti-GluR2/3 staining, eyes were hemisected by a scalpel blade (No.11, Feather) and mounted with the OPL perpendicular to the cover slip.

Confocal image stacks were acquired on a FV1000 (Olympus) microscope using a 1.35 NA 60× oil-immersion or 0.85 NA 20× oil-immersion objective lenses. Images were typically acquired with an XY resolution of 0.077 μm/pixel and 0.25 μm-thick Z slices for H3 HCs, and with an XY resolution of 0.462 μm/pixels and 1 μm-thick Z slices for whole eyes.

Image analysis

Stack images were median-filtered in Matlab (Mathwork) and 3D-reconstructed in Amira (Mercury Computer Systems). To view the H3 HCs dendritic arbors in the ‘top view’, the 3D–reconstructed image was oriented with the OPL parallel to the viewing perspective. The ‘side view’ was generated by orienting the OPL perpendicular to the viewing perspective, and thinly sliced digitally using the oblique slice function in Amira. Dendritic tip invaginations into cones were determined by examining side views throughout the dendritic arbor of the HC.

Connectivity maps were obtained by marking morphologically identified tip invaginations into cones on the maximum intensity projection of the H3 HC dendritic arbor. Dendritic field size and synapse distributions were measured from the connectivity maps using Fiji[53]. The locations of UV and blue cone terminal were marked on the connectivity maps and the total numbers of UV and blue cones within dendritic field were counted. The percentages of cones contacted within the dendritic field were obtained by dividing the number of UV or blue cones contacted by the total number of UV or blue cones within the dendritic field. Colabeling of transgenic fluorescent labels and immunofluorescence from anti-UV- or blue-opsin staining was analyzed using the masking function in Amira. Labeled cones were counted in Fiji using the maximum intensity projections of cells from Amira 3D reconstructions of whole eyes. Line-scans of pixel intensity in Figure 4 were obtained from side views of H3 HCs and cones using the MetaMorph (Universal Imaging) line-scan

function with 10 pt line thickness. Images in the figures were further processed in Photoshop (Adobe) by adjusting brightness, contrast and hues.

Statistical analysis

We used the Wilcoxon-Mann-Whitney rank sum test for comparisons of synapse numbers, dendritic field size, tip density, total tip number, percentage of cones contacted and UV/blue synapse ratios. (Figures 1d, 3c, 5i–l, 6i–l, 8m–o, 9e–f, Supplementary Fig. 1, Supplementary Fig. 2b and Supplementary Fig. 6) A one-way ANOVA was used to test for differences in the number of synapse across ages in Figure 2b and for the dendritic field size in Figure 3b. The Pearson correlation coefficient was calculated for the regression fit of the data points in Figure 7d.

Electron microscopy

Briefly, zebrafish larvae were fixed in 4% glutaraldehye in 0.1 M sodium cacodylate buffer, pH 7.4 for several hours, washed in buffer three times and placed in 1% osmium tetroxide in buffer. Tissue was dehydrated in a graded series of alcohol, embedded in resin, sectioned and imaged[19]

Supplementary Material

Refer to Web version on PubMed Central for supplementary material.

Acknowledgements

We thank S. Kawamura for providing *Tg(sws1:GFP)* and *Tg(sws2:GFP)* transgenic fish, and D.R. Hyde and J. Nathans for providing UV- and blue-opsin antibodies. We also thank Wong lab members for helpful discussions and critical reading of the manuscript. This study is supported by NIH grants EY14358 to R.O.W., EY015509 to P.A.R., the Vision Core Grant EY01730, the Vision Training Grant EY07031 and Developmental Biology Grant HD07183 to F.D.D., Natural Sciences and Engineering Research Council of Canada to W.T.A., Uehara Memorial Foundation to T.Y. and S.C.S.

REFERENCES

1. Williams ME, de Wit J, Ghosh A. Molecular mechanisms of synaptic specificity in developing neural circuits. Neuron. 2010; 68:9–18. [PubMed: 20920787]
2. Sanes JR, Yamagata M. Many paths to synaptic specificity. Annu. Rev. Cell Dev. Biol. 2009; 25:161–195. [PubMed: 19575668]
3. Witter MP. Organization of the entorhinal-hippocampal system: a review of current anatomical data. Hippocampus. 1993:33–44. p3 Spec No. [PubMed: 8287110]
4. Shen K, Scheiffele P. Genetics and cell biology of building specific synaptic connectivity. Annu. Rev. Neurosci. 2010; 33:473–507. [PubMed: 20367446]
5. Pasterkamp RJ. Getting neural circuits into shape with semaphorins. Nat. Rev. Neurosci. 2012; 13:605–618. [PubMed: 22895477]
6. Hruska M, Dalva MB. Ephrin regulation of synapse formation, function and plasticity. Mol. Cell. Neurosci. 2012; 50:35–44. [PubMed: 22449939]
7. Ding JB, Oh W-J, Sabatini BL, Gu C. Semaphorin 3E–Plexin-D1 signaling controls pathway-specific synapse formation in the striatum. Nat. Neurosci. 2012; 15:215–223. [PubMed: 22179111]
8. Wässle H. Parallel processing in the mammalian retina. Nat. Rev. Neurosci. 2004; 5:747–757. [PubMed: 15378035]

9. Dacheux RF, Chimento MF, Amthor FR. Synaptic input to the on-off directionally selective ganglion cell in the rabbit retina. J. Comp. Neurol. 2003; 456:267–278. [PubMed: 12528191]
10. Famiglietti EV. Synaptic organization of complex ganglion cells in rabbit retina: type and arrangement of inputs to directionally selective and local-edge-detector cells. J. Comp. Neurol. 2005; 484:357–391. [PubMed: 15770656]
11. Schwartz GW, et al. The spatial structure of a nonlinear receptive field. Nat. Neurosci. 2012; 15:1572–1580. [PubMed: 23001060]
12. Li YN, Tsujimura T, Kawamura S, Dowling JE. Bipolar cell-photoreceptor connectivity in the zebrafish (Danio rerio) retina. J. Comp. Neurol. 2012; 520:3786–3802. [PubMed: 22907678]
13. Nawrocki L, BreMiller R, Streisinger G, Kaplan M. Larval and adult visual pigments of the zebrafish, Brachydanio rerio. Vision Res. 1985; 25:1569–1576. [PubMed: 3832580]
14. Robinson J, Schmitt EA, Hárosi FI, Reece RJ, Dowling JE. Zebrafish ultraviolet visual pigment: absorption spectrum, sequence, and localization. Proc. Natl. Acad. Sci. U. S. A. 1993; 90:6009–6012. [PubMed: 8327475]
15. Song PI, Matsui JI, Dowling JE. Morphological types and connectivity of horizontal cells found in the adult zebrafish (Danio rerio) retina. J. Comp. Neurol. 2008; 506:328–338. [PubMed: 18022944]
16. Li YN, Matsui JI, Dowling JE. Specificity of the horizontal cell-photoreceptor connections in the zebrafish (Danio rerio) retina. J. Comp. Neurol. 2009; 516:442–453. [PubMed: 19655401]
17. Connaughton VP, Nelson R. Spectral responses in zebrafish horizontal cells include a tetraphasic response and a novel UV-dominated triphasic response. J. Neurophysiol. 2010; 104:2407–2422. [PubMed: 20610786]
18. Shields CR, et al. Retinal horizontal cell-specific promoter activity and protein expression of zebrafish connexin 52.6 and connexin 55.5. J. Comp. Neurol. 2007; 501:765–779. [PubMed: 17299759]
19. Williams PR, et al. In vivo development of outer retinal synapses in the absence of glial contact. J. Neurosci. 2010; 30:11951–11961. [PubMed: 20826659]
20. Biehlmaier O, Neuhauss SCF, Kohler K. Synaptic plasticity and functionality at the cone terminal of the developing zebrafish retina. J. Neurobiol. 2003; 56:222–236. [PubMed: 12884262]
21. Neuhauss SC, et al. Genetic disorders of vision revealed by a behavioral screen of 400 essential loci in zebrafish. J. Neurosci. 1999; 19:8603–8615. [PubMed: 10493760]
22. Vihtelic TS, Doro CJ, Hyde DR. Cloning and characterization of six zebrafish photoreceptor opsin cDNAs and immunolocalization of their corresponding proteins. Vis. Neurosci. 1999; 16:571–585. [PubMed: 10349976]
23. Allison WT, et al. Ontogeny of cone photoreceptor mosaics in zebrafish. J. Comp. Neurol. 2010; 518:4182–4195. [PubMed: 20878782]
24. Suzuki SC, et al. Cone photoreceptor types in zebrafish are generated by symmetric terminal divisions of dedicated precursors. Proc. Natl. Acad. Sci. U. S. A. 2013; 110:15109–15114. [PubMed: 23980162]
25. Alvarez-Delfin K, et al. Tbx2b is required for ultraviolet photoreceptor cell specification during zebrafish retinal development. Proc. Natl. Acad. Sci. U. S. A. 2009; 106:2023–2028. [PubMed: 19179291]
26. Schiavo G, et al. Tetanus and botulinum-B neurotoxins block neurotransmitter release by proteolytic cleavage of synaptobrevin. Nature. 1992; 359:832–835. [PubMed: 1331807]
27. Turrigiano GG, Nelson SB. Homeostatic plasticity in the developing nervous system. Nat. Rev. Neurosci. 2004; 5:97–107. [PubMed: 14735113]
28. Hashimoto K, Kano M. Synapse elimination in the developing cerebellum. Cell. Mol. Life Sci. Cmls. 2013
29. Vitureira N, Letellier M, Goda Y. Homeostatic synaptic plasticity: from single synapses to neural circuits. Curr. Opin. Neurobiol. 2012; 22:516–521. [PubMed: 21983330]
30. Morgan JL, Soto F, Wong ROL, Kerschensteiner D. Development of cell type-specific connectivity patterns of converging excitatory axons in the retina. Neuron. 2011; 71:1014–1021. [PubMed: 21943599]

31. Guido W. Refinement of the retinogeniculate pathway. J. Physiol. 2008; 586:4357–4362. [PubMed: 18556365]
32. Malun D, Brunjes PC. Development of olfactory glomeruli: temporal and spatial interactions between olfactory receptor axons and mitral cells in opossums and rats. J. Comp. Neurol. 1996; 368:1–16. [PubMed: 8725290]
33. Branchek T. The development of photoreceptors in the zebrafish brachydanio rerio. II Function. J. Comp. Neurol. 1984; 224:116–122. [PubMed: 6715575]
34. Hu M, Easter SS. Retinal neurogenesis: the formation of the initial central patch of postmitotic cells. Dev. Biol. 1999; 207:309–321. [PubMed: 10068465]
35. Raven MA, Oh ECT, Swaroop A, Reese BE. Afferent control of horizontal cell morphology revealed by genetic respecification of rods and cones. J. Neurosci. 2007; 27:3540–3547. [PubMed: 17392470]
36. Crepel F, Delhaye-Bouchaud N, Dupont JL. Fate of the multiple innervation of cerebellar Purkinje cells by climbing fibers in immature control, x-irradiated and hypothyroid rats. Brain Res. 1981; 227:59–71. [PubMed: 7470934]
37. Bravin M, Rossi F, Strata P. Different climbing fibres innervate separate dendritic regions of the same Purkinje cell in hypogranular cerebellum. J. Comp. Neurol. 1995; 357:395–407. [PubMed: 7673475]
38. Rossi F, van der Want JJ, Wiklund L, Strata P. Reinnervation of cerebellar Purkinje cells by climbing fibres surviving a subtotal lesion of the inferior olive in the adult rat. II. Synaptic organization on reinnervated Purkinje cells. J. Comp. Neurol. 1991; 308:536–554. [PubMed: 1865016]
39. Sanes JR, Lichtman JW. Development of the vertebrate neuromuscular junction. Annu. Rev. Neurosci. 1999; 22:389–442. [PubMed: 10202544]
40. Katz LC, Crowley JC. Development of cortical circuits: lessons from ocular dominance columns. Nat. Rev. Neurosci. 2002; 3:34–42. [PubMed: 11823803]
41. Cesa R, Strata P. Axonal competition in the synaptic wiring of the cerebellar cortex during development and in the mature cerebellum. Neuroscience. 2009; 162:624–632. [PubMed: 19272433]
42. Kano M, et al. Persistent multiple climbing fiber innervation of cerebellar Purkinje cells in mice lacking mGluR1. Neuron. 1997; 18:71–79. [PubMed: 9010206]
43. Miyazaki T, et al. Cav2.1 in cerebellar Purkinje cells regulates competitive excitatory synaptic wiring, cell survival, and cerebellar biochemical compartmentalization. J. Neurosci. 2012; 32:1311–1328. [PubMed: 22279216]
44. She K, Craig AM. NMDA receptors mediate synaptic competition in culture. Plos One. 2011; 6:e24423. [PubMed: 21935408]
45. Kerschensteiner D, Morgan JL, Parker ED, Lewis RM, Wong ROL. Neurotransmission selectively regulates synapse formation in parallel circuits in vivo. Nature. 2009; 460:1016–1020. [PubMed: 19693082]
46. Li H, Chuang AZ, O'Brien J. Photoreceptor coupling is controlled by connexin 35 phosphorylation in zebrafish retina. J. Neurosci. 2009; 29:15178–15186. [PubMed: 19955370]
47. Takechi M, Hamaoka T, Kawamura S. Fluorescence visualization of ultraviolet-sensitive cone photoreceptor development in living zebrafish. Febs Lett. 2003; 553:90–94. [PubMed: 14550552]
48. Takechi M, Seno S, Kawamura S. Identification of cis-acting elements repressing blue opsin expression in zebrafish UV cones and pineal cells. J. Biol. Chem. 2008; 283:31625–31632. [PubMed: 18796431]
49. Salbreux G, Barthel LK, Raymond PA, Lubensky DK. Coupling mechanical deformations and planar cell polarity to create regular patterns in the zebrafish retina. Plos Comput. Biol. 2012; 8:e1002618. [PubMed: 22936893]
50. Ren JQ, McCarthy WR, Zhang H, Adolph AR, Li L. Behavioral visual responses of wild-type and hypopigmented zebrafish. Vision Res. 2002; 42:293–299. [PubMed: 11809482]
51. Godinho L, et al. Nonapical symmetric divisions underlie horizontal cell layer formation in the developing retina in vivo. Neuron. 2007; 56:597–603. [PubMed: 18031679]

52. Kwan KM, et al. The Tol2kit: a multisite gateway-based construction kit for Tol2 transposon transgenesis constructs. Dev. Dyn. 2007; 236:3088–3099. [PubMed: 17937395]

53. Schindelin J, et al. Fiji: an open-source platform for biological-image analysis. Nat. Methods. 2012; 9:676–682. [PubMed: 22743772]

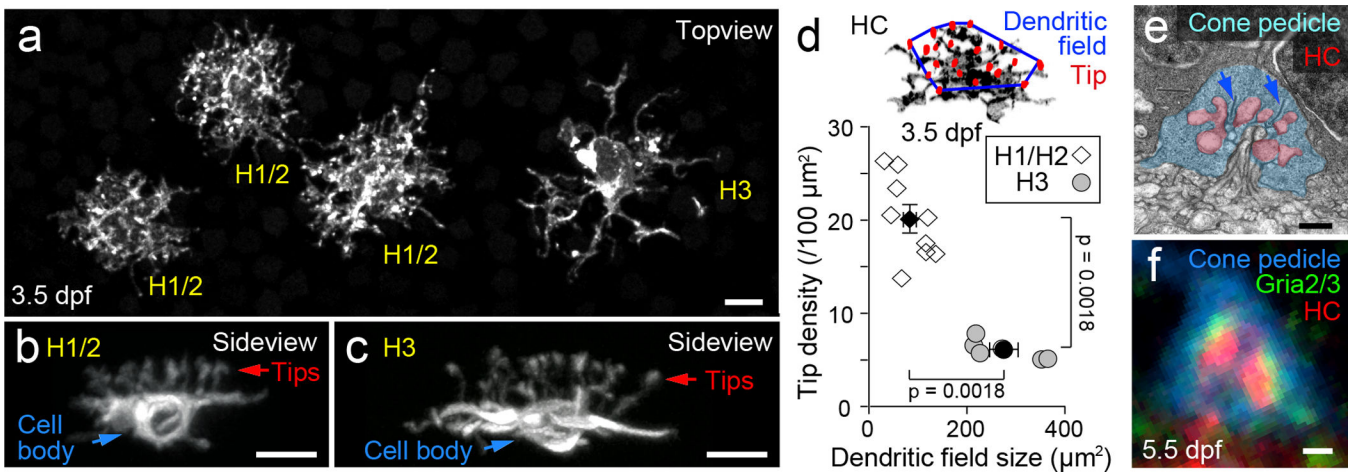

Figure 1. Morphology of HCs in larval zebrafish retina

(**a**) Examples of HCs at 3.5 days postfertilization (dpf) visualized by injecting plasmid DNA (see Methods for details) into fertilized eggs. Shown here is the maximum intensity projection of a confocal image stack of the back of an isolated eye. (**b,c**) Orthogonal views of two-photon reconstructions of cone HCs in live fish (3.5 dpf). Dendritic tips extending from the HCs are clearly visible from these side views. Scale bars (a–c): 5 µm. (**d**) Tip density plotted against dendritic field size of morphologically classified H1/2 and H3 HCs at 3.5 dpf. The dendritic field is defined as the area encompassed by a convex polygon whose corners touch the outer most dendritic tips. Each open or gray symbol represents a cell. Black symbols and error bars represent means and S.E.M. p-values from Wilcoxon-Mann-Whitney rank sum test. n=9 for H1/2 and n=6 for H3. (**e**) EM image of a cone pedicle showing invaginating HC dendritic tips (red) that are apposed to characteristic pre-synaptic ribbons, sites of transmitter release (arrows). (**f**) Single plane confocal image showing Gria2/3 (also known as GluR2/3) immunoreactive puncta (green) colocalized with a HC dendritic tip (red) within a cone pedicle (blue). Scale bar (e,f): 0.5 µm.

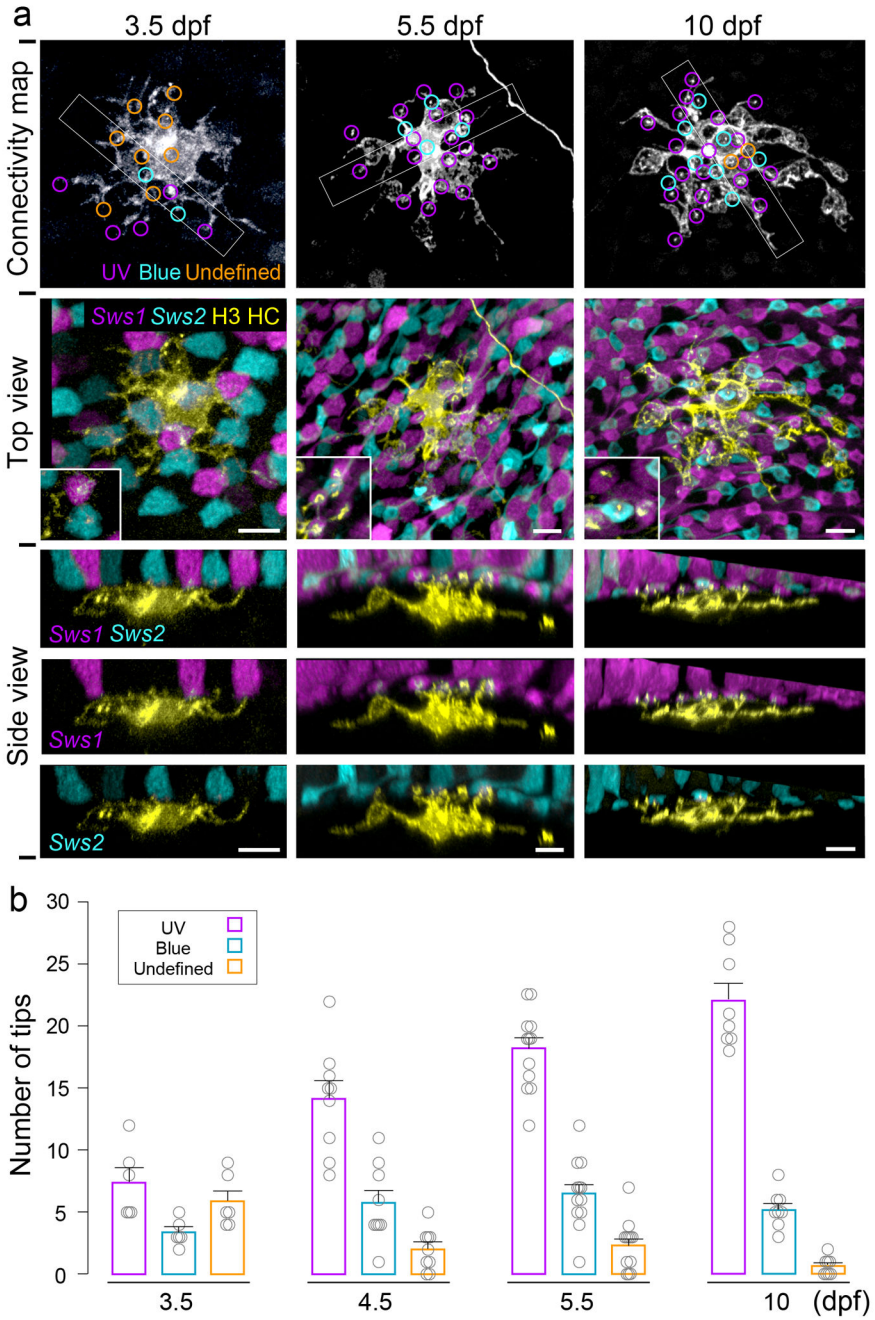

Figure 2. Connectivity patterns of H3 HCs across development

(**a**) Examples of larval H3 HCs transiently expressing fluorescent protein in the background of *Tg*(*sws1:GFP; sws2:mCherry*). Shown are maximum intensity projections or orthogonal views through a small part of the arbor. Insets in top view panels show higher magnifications of dendritic tips invaginating into a cone pedicle. Open circles map the locations of dendritic tips that contacted UV or blue cones in the double transgenic line (magenta or blue circles respectively), as judged from 3D reconstructions of the cell and its surrounding cones. Some tips (orange circles, undefined) could not be assigned to either UV

or blue cones. Scale bars: 5 μm. (**b**) Population data showing the mean number of UV or blue cone-associated tips and undefined tips made by H3 HCs in the background of *Tg*(*sws1:GFP; sws2:mCherry*) fish. Each open circle represents one cell. n=6 for 3.5 dpf, n=9 for 4.5 dpf, n=12 for 5.5 dpf, n=8 for 10 dpf. Error bars are S.E.M.

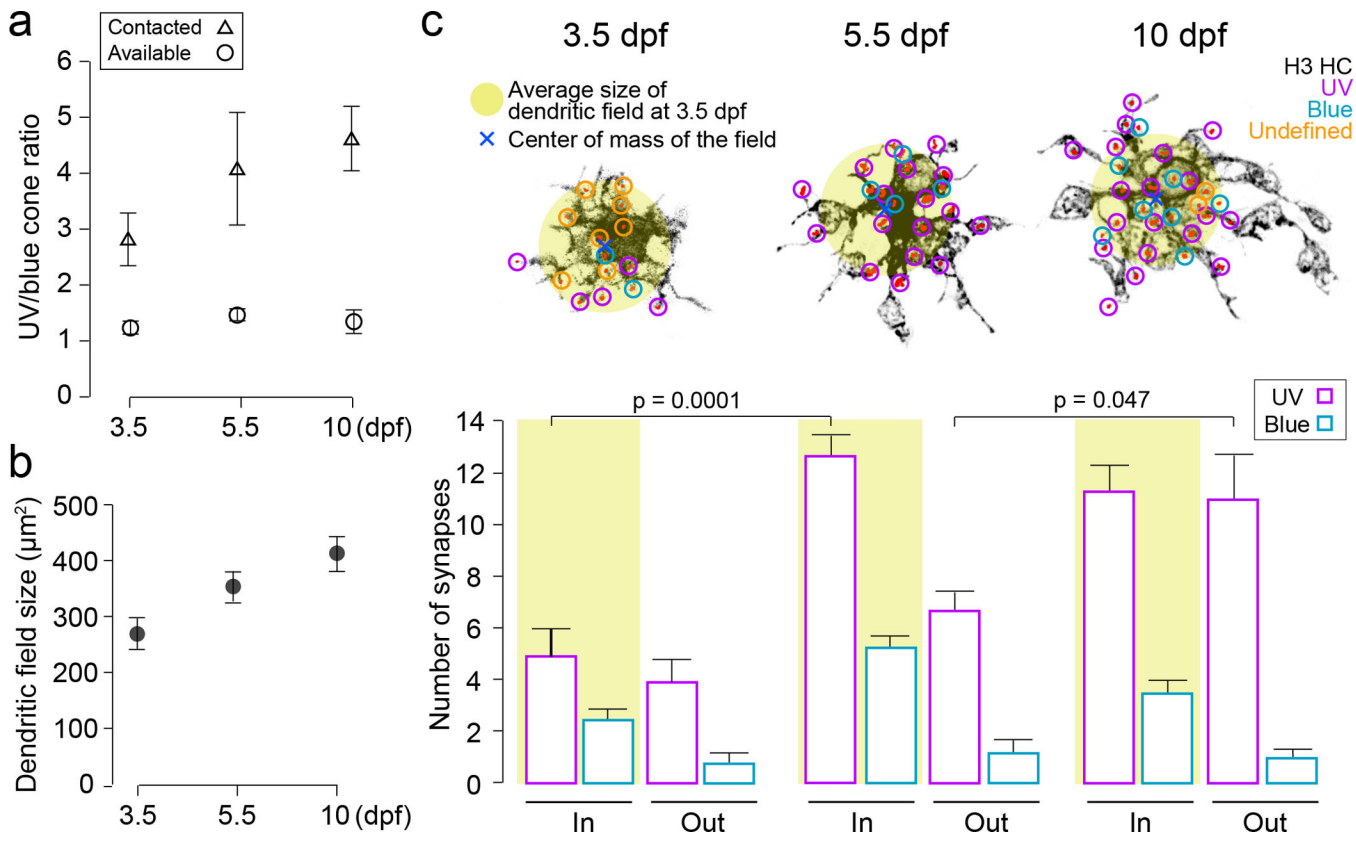

Figure 3. Developmental increase in UV:blue cone synapse ratio occurs by selective addition of UV cone connections

(**a**) Plots across ages of the mean ratio of the UV:blue cones available (circles) as well as the adjusted mean ratio of UV:blue cones that are contacted by H3 HCs (triangles). Contacted (n=6 for 3.5 dpf, n=12 for 5.5 dpf, n=8 for 10 dpf); available (n=4 for all ages). (**b**) Mean H3 HC dendritic field sizes at different ages. (**c**) (Upper panel) Connectivity maps of example H3 HCs at different ages. A circle (yellow) with an area equivalent to the average 3.5 dpf H3 HC dendritic field size was centered on the center of mass of the dendritic field. (Lower panel) The mean numbers of UV and blue cone synapses within (In) or outside (Out) the yellow-filled circle were plotted for cells reconstructed at different ages. In general, synapses added outside the circle largely represent addition of synapses to the dendrites that grew after 3.5 dpf. In all panels, UV and blue cone synapse numbers obtained from FP expression in transgenic fish were adjusted according to the values of % transgenic expression per opsin expression from Supplementary Fig. 2. All error bars are S.E.M. p-values from Wilcoxon-Mann- Whitney rank sum test. n=6 for 3.5 dpf, n=9 for 5.5 dpf, n=8 for 10 dpf in (b,c).

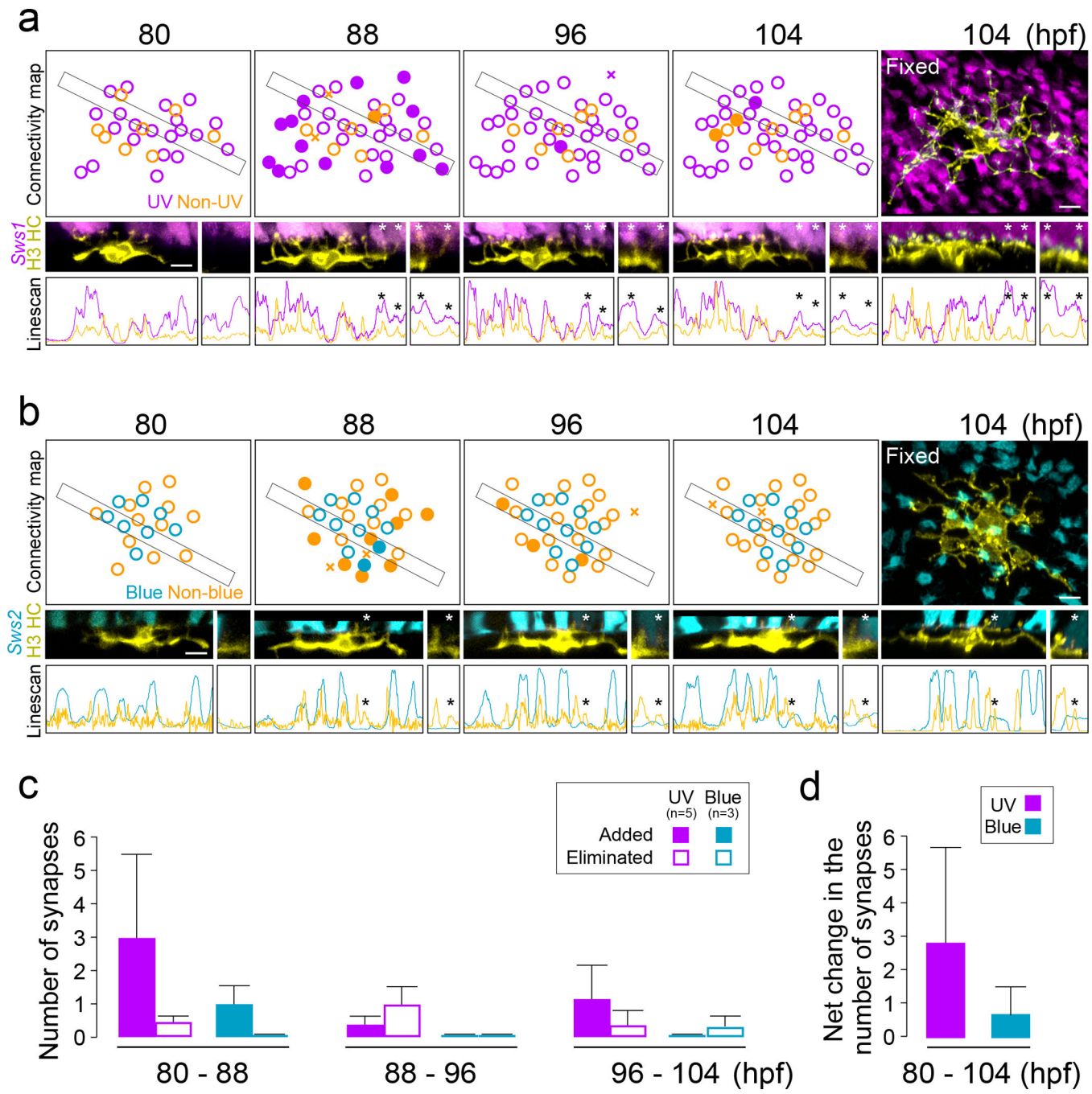

Figure 4. Dynamic H3 HC processes selectively target UV cones

(**a,b**) Multiphoton time-lapse imaging of an H3 HC in the background of (a) *Tg*(*sws1:GFP*) or (b) *Tg*(*sws2:GFP*). For each time point, an orthogonal view of the cell and labeled cones within the boxed region is provided below the connectivity map. A line-scan of this region showing the relative pixel intensities of the two channels (violet, UV cone signal or cyan, blue cone signal; yellow, HC signal) is presented below the view of the cell. Asterisks mark the location where, over time, a dendritic tip emerged and contacted UV or blue cones. Higher magnification of this location is shown on the right panels. A confocal reconstruction

of the cell after fixation at the final time-point (104 hpf) clearly identifies the formation of new synapses. In the connectivity maps, solid circles represent synapses added in-between time points; open circles are stable contacts and X indicates eliminated contacts. Scale bars: 5 μm. (**c**) Population data showing the mean number of UV and blue cone synapses added and eliminated during the time course of multiphoton imaging. (**d**) Net change in the number of UV and blue cone synapses (n=5 for UV and n=3 for blue). Error bars are S.E.M.

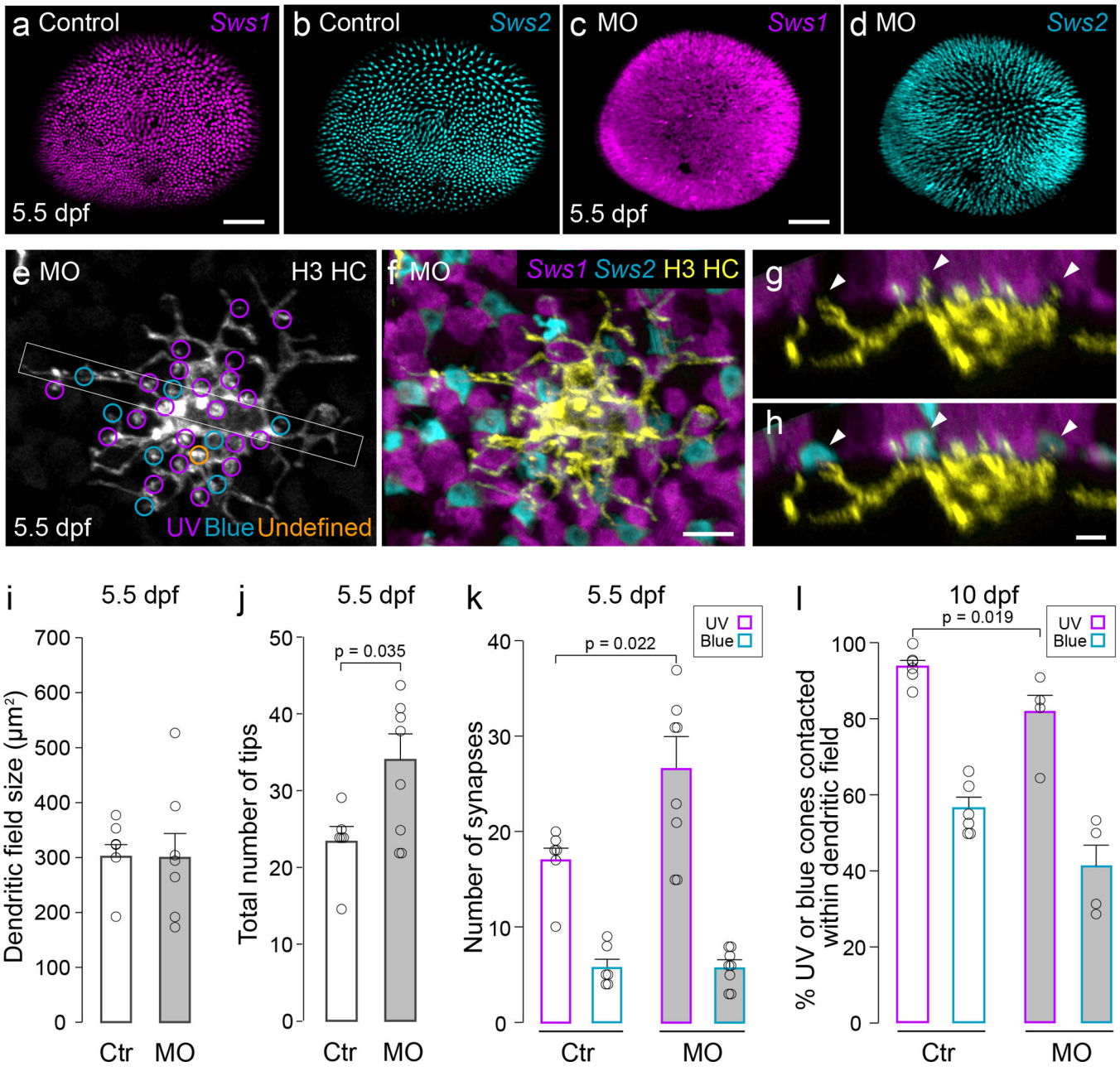

Figure 5. Increasing UV cone availability leads to more UV cone synapses without affecting blue cone synapse number

(**a**–**d**) Maximum intensity projections of confocal image stacks of wholemount eyes in the background of *Tg*(*sws1:GFP; sws2:mCherry*). UV and blue cone distributions are shown for standard morpholino injected animals (a and b; control) and in *thrb* morphants (MO). Scale bars: 50 µm. (**e**–**h**) Example of an H3 HC visualized in *thrb* MO, and its connectivity map. Arrowheads in the oblique view of the cell (**g,h**) indicate dendritic tips invaginating blue cones. Scale bars: 5 µm. (**i**–**l**) Population data comparing mean measurements in control (ctr) and *thrb* MO (MO). See Methods for details of analysis. Each open circle represents one H3 HC. Error bars are S.E.M. p-values from Wilcoxon-Mann-Whitney rank sum test.

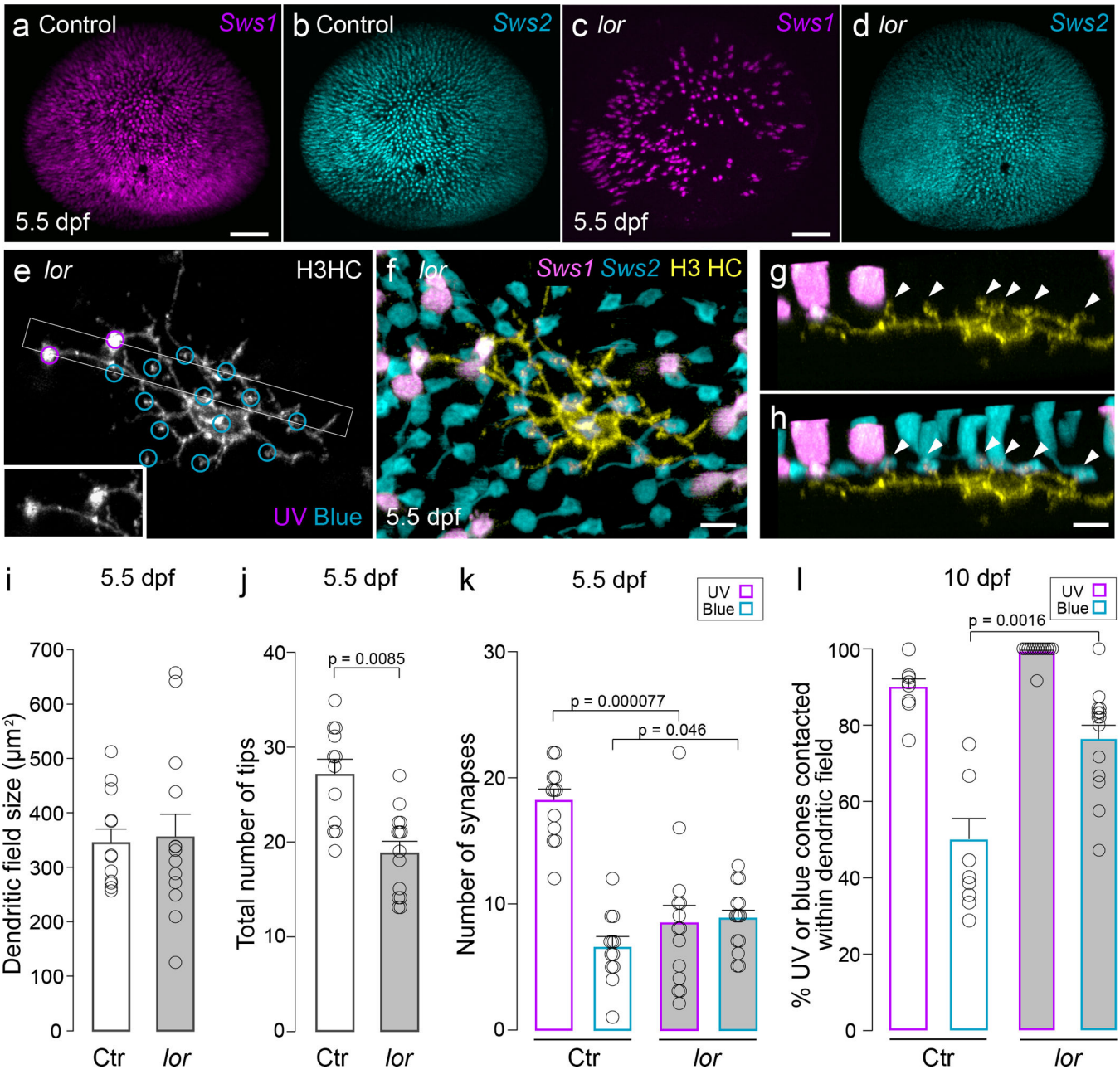

Figure 6. H3 HCs increase synaptogenesis with blue cones in the absence of UV cones

(**a**–**d**) Maximum intensity projections of confocal image stacks of wholemount eyes in the background of *Tg(sws1:GFP; sws2:mCherry)*. UV and blue cone distributions are shown for wildtype animals (a and b; control) and in the *lor* mutant *(lor)*. Scale bars: 50 µm. (**e**–**h**) Example of an H3 HC visualized in *lor*, and its connectivity map. Inset in (**e**) shows a higher magnification view of enlarged dendritic tips within UV cones. Arrowheads in the orthogonal view of the cell (**g**,**h**) indicate dendritic tips invaginating blue cones. Scale bars: 5 µm. Note that in Figure 7, some UV cones in *lor* receive more than 1 dendritic invagination from the same HC. We counted these tips as a separate ‘synapse’. (**i**–**l**) Summary of mean measurements in control (ctr) and *lor*. See Methods for details of

analysis. Each open circle represents one H3 HC. Error bars are S.E.M. p values from Wilcoxon-Mann-Whitney rank sum test.

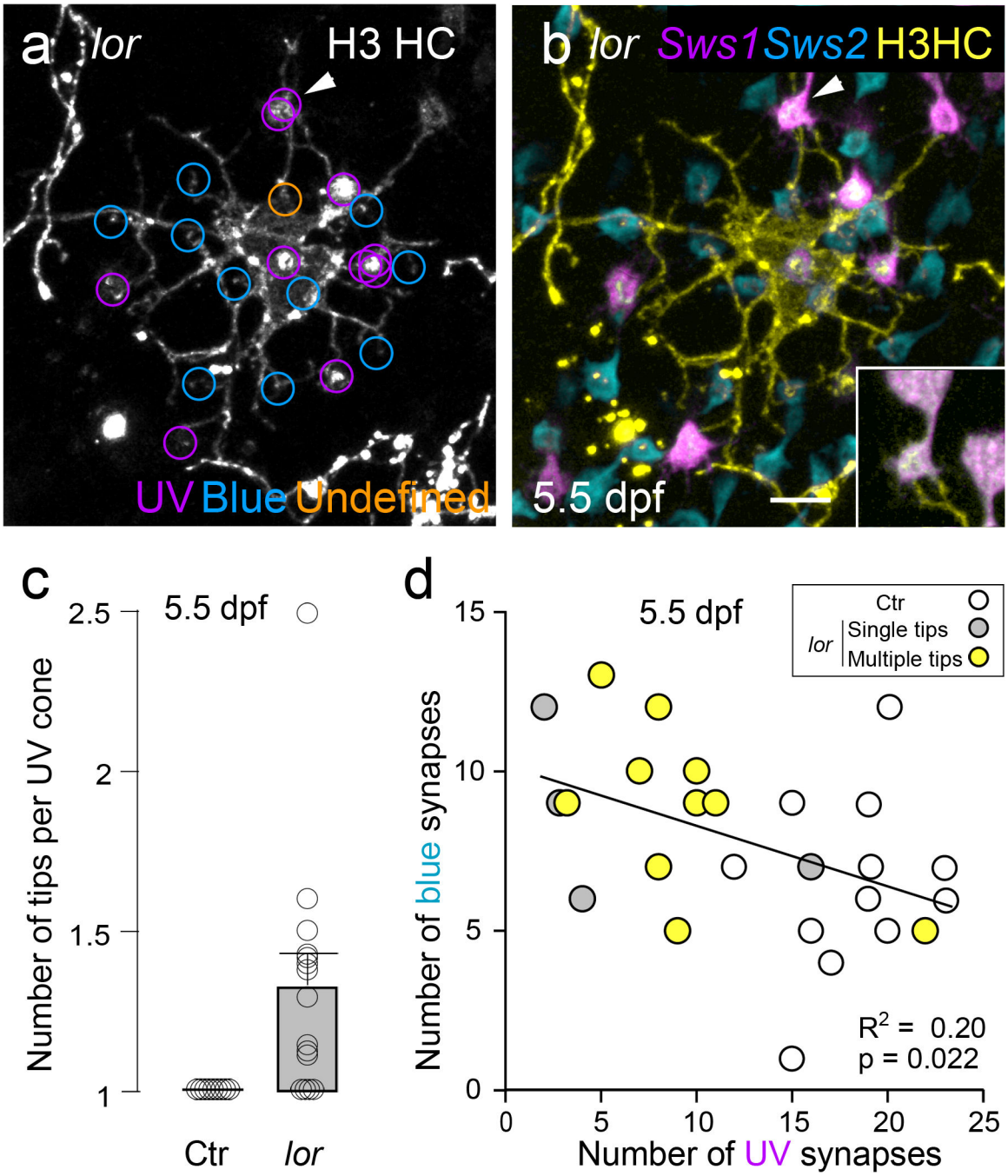

Figure 7. Inverse correlation between the number of UV and blue cones synapsing with H3 HCs in l or mutants

(**a**,**b**) An example of an H3 HC labeled in *Tg(sws1:GFP; sws2:mCherry)* crossed in the *lor* background. Connectivity map is shown in (**a**). Arrowhead indicates an unusual invagination into a UV cone by two dendritic tips from the same HC. Dendritic tips of larval H3 HCs normally do not show such branching or co-innervation of the same pedicle. Scale bar: 5 μm. An inset shows High-magnification view of the tip indicated by the arrowhead. (**c**) Quantification of the mean number of dendritic tips invaginating a single UV cone in

wildtype (ctr) and *lor*. Open circles represent the average value for individual H3 HCs. Error bars are S.E.M. (**d**) The number of blue and UV cones synapsing a given H3 HC (each circle) at 5.5 dpf are plotted here for wildtype (ctr) and *lor* mutants. All control H3 HCs had a single dendritic invagination into a cone pedicle. In *lor*, however, some H3 HCs project two or more dendritic tips into the cone pedicle (multiple tips). R-square and p-value from Pearson correlation coefficient.

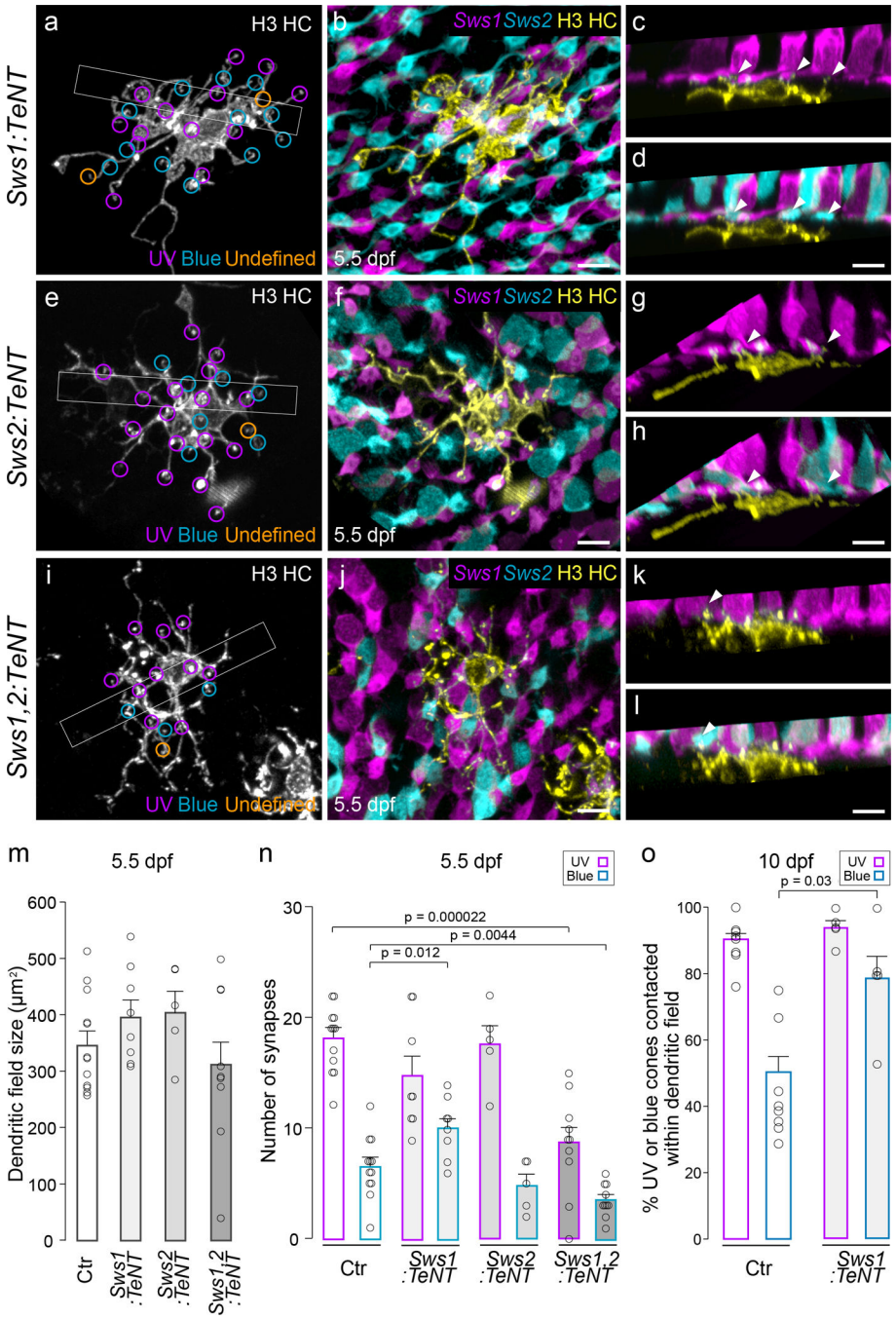

Figure 8. UV cone transmission regulates blue cone synapse number

(**a**–**l**) Examples of H3 HCs and their connectivity maps in the background of *Tg(sws1:TeNT; sws2:mCherry)* (**a-d**), *Tg*(*sws1:GFP; sws2:TeNT*) (**e**–**h**), or *Tg*(*sws1:TeNT; sws2:TeNT; sws2:mCherry*) (**i**–**l**). Sideviews of rectangular regions outlined in (**a,e,i**) are shown in (**c,d,g,h,k,l**). Arrowheads indicate blue cone synapses. Scale bars: 5 µm. (**m**–**o**) Comparison of mean measurements across conditions. See Methods for details of analysis. Control animals (ctr). Each open circle represents one H3 HC. Error bars are S.E.M. p-values from Wilcoxon-Mann-Whitney rank sum test.

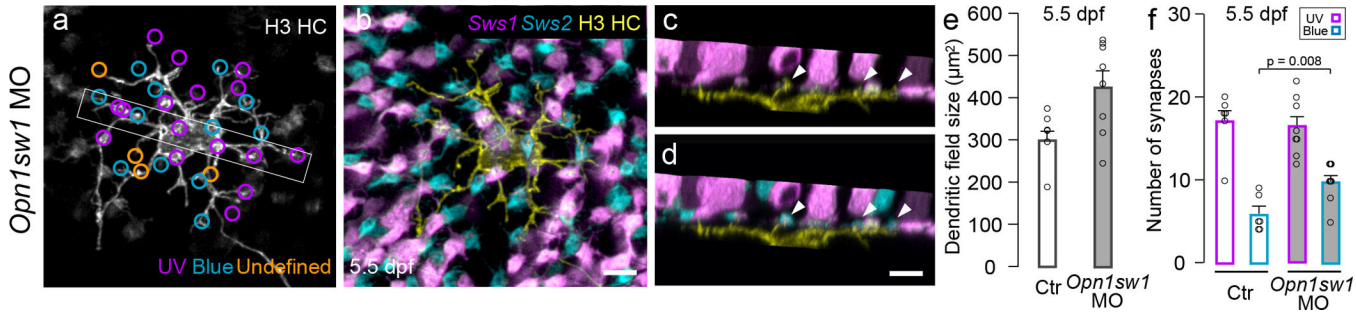

Figure 9. UV light-driven transmission regulates H3 HC connectivity with blue cones

(**a**–**d**) An H3 HC and its connectivity map in the background of a *Tg*(*sws1:GFP; sws2:mCherry*) fish that was injected with a morpholino against UV-opsin (*Opn1sw1* MO). Arrows indicate blue cone synapses. Scale bars: 5 µm. Comparison of measurements between standard morpholino (ctr) and *Opn1sw1* morpholino injected animals. Each open circle represents one H3 HC. (**e**, **f**) Comparison of mean measurements across conditions. Control animals (ctr). See Methods for details of analysis. Each open circle represents one H3 HC. Error bars are S.E.M. p values from Wilcoxon-Mann-Whitney rank sum test.